Design of singularity-free fixed-time fault-tolerant control for HFVs with guaranteed asymmetric time-varying flight state constraints

Zuo, Renwei; Li, Yinghui; Lv, Maolong; Liu, Zongcheng; Dong, Zehong

Important note
To cite this publication, please use the final published version (if applicable).
Please check the document version above.

Design of singularity-free fixed-time fault-tolerant control for HFVs with guaranteed asymmetric time-varying flight state constraints

Renwei Zuo [a], Yinghui Li [b], Maolong Lv [c,d,*], Zongcheng Liu [b], Zehong Dong [a]

[a] *College of Graduate, Air Force Engineering University, Xi'an 710038, China*
[b] *College of Aeronautics Engineering, Air Force Engineering University, Xi'an 710038, China*
[c] *College of Air Traffic Control and Navigation, Air Force Engineering University, Xi'an 710038, China*
[d] *Delft Center for Systems and Control, Delft University of Technology, Mekelweg 2, Delft 2628CD, the Netherlands*

ARTICLE INFO

ABSTRACT

This article solves the fixed-time trajectory tracking problem for hypersonic flight vehicles (HFVs) encountered with diverse actuator faults and asymmetric envelope constraints. In contrast to the state of the art, the crucial characteristics of our design lie in obviating the explosion of complexity of the conventional recursive design, and in realizing satisfactory preselected tracking qualities for flight states in the sense of guaranteeing asymmetric envelope constraints. More precisely, by exploiting the fixed-time command filters to produce certain command signals and their derivatives, a modified command-filtered control algorithm is formulated to circumvent heavy computation burden caused by repetitive derivative of intermediate control laws. A two-step control methodology is devised based on an auxiliary compensating dynamics, which is capable of compensating for the actuator faults completely without the need for prior knowledge about the lumped disturbances and the actuator faults. Time-varying asymmetric barrier Lyapunov functions are introduced to confine the flight state tracking errors within the corresponding time-varying compact sets all the time provided their initial values remain therein. The effectiveness of the proposed method is validated by comparative simulation results.

1. Introduction

Hypersonic flight vehicles (HFVs) emerge as the times require for their capability of hypersonic cruise without carrying any oxidizer, viewed as the essential step towards achieving routine space access and remote power projection [1–8]. To improve the control performances of HFVs in terms of complicated flight conditions and time-varying aerodynamic coefficients, it is crucial to implement the state-of-the-art control approaches, e.g., sliding mode control [9–11], fault-tolerant control [12,13], dynamic inversion control [14], adaptive backstepping control [15–17], and so on. Among them, adaptive backstepping control has aroused enormous attention and interest owing to its broad application scope [18–21]. However, implementation of adaptive backstepping controllers inevitably suffers from the explosion of complexity associated with the repeated differentiation of virtual control signal. It is well-recognized that analytic calculation of these derivatives becomes overly cumbersome in applications as the order of a nonlinear system increases [22].

To obviate the requirement of analytic differentiation, the paradigm of command-filtered backstepping was originally proposed in [23], where some command filters are resorted to estimate the differential coefficient of the virtual controllers [24]. Nonetheless, preliminary versions of the command-filtered backstepping are almost asymptotically stable methodologies [25], which indicates that the closed-loop convergence is achieved as time goes to infinity. In view of high speed and agile maneuvering of HFVs, fast convergence and strong robustness are essential for control design in the hypersonic regime. Taking advantage of faster response, higher tracking precision and better disturbance-rejection ability, the so-called finite-time [26–29] or fixed-time tracking concepts [30] have been widely investigated with the preassigned beforehand convergence rate. To be specific, fixed-time control has a prominent superiority that its convergence time is upper bounded by a positive constant irrelevant to the initial conditions [30,31]. However, the extant accomplishments of fixed-time

* Corresponding author at: College of Air Traffic Control and Navigation, Air Force Engineering University, Xi'an 710038, China.
E-mail address: M.Lyu@tudelft.nl (M. Lv).

control schemes possess the potential singularity issue, which is inherent in the non-differentiable virtual control signal as the tracking error approaches zero.

Stemming from the viewpoint of engineering, the tightly integrated airframe-engine design leads to the strong aero-propulsion coupling, consequently limiting the angle of attack (AOA) and flight path angle (FPA) within the narrow permissible ranges. It must be emphasized that the transgression of these envelope constraints probably results in a disastrous phenomenon, known as inlet unstart. Although the envelope constraints have been extensively explored relying on the multiple-type barrier Lyapunov function (BLF), e.g., log-type BLF [32–35], integral-type BLF [36], and tan-type BLF [37], these barriers do not take into account possibly asymmetry in the operating regions of HFVs. More precisely, the AOA and FPA cannot operate in symmetric regions owing to the physics of a plane when climbing or descending. To summarize, we aim to propose a fixed-time command-filtered trajectory tracking control methodology for HFVs subject to diverse actuator faults and asymmetric envelope constraints. The main contributions of this article are four-fold:

- A novel adaptive command-filtered control methodology is presented by employing a fixed-time command filter, which is capable of estimating the differential coefficient of the virtual controller within fixed time.
- With the aid of a piecewise but differentiable switching control law that guarantees the continuity and differentiability everywhere via an appropriate design, the singularity issue that exists in [30,31] is effectively evaded in our work.
- Time-varying asymmetric barrier Lyapunov functions are appropriately embedded into the control design which are shown to confine the flight state variables within some asymmetric and time-varying sets all the time, provided that the initial conditions are inside of corresponding sets.
- Thanks to the introduction of an auxiliary compensating dynamics counteracting the adverse effects caused by actuator faults, the proposed two-step fault-tolerant control methodology not only ensures the boundedness of closed-loop signals but can also preserve the validity of fixed-time command filters.

The remainder of this work is organized as follows. The vehicle model and problem formulation are described in Section 2. The fixed-time command-filtered control methodology is developed in Section 3. In Section 4, we provide the stability analysis for the whole HFVs dynamics. Section 5 presents the comparative simulation tests of the proposed control in contrast to the extant results. Finally, Section 6 concludes the paper.

2. The vehicle model and problem formulation

2.1. Hypersonic flight vehicle dynamics

The longitudinal motion of flexible HFVs is given by a set of differential equations for rigid-body states $[V, h, \gamma, \alpha, Q]^\top$ and flexible states $\boldsymbol{\eta} = [\eta_1, \dot{\eta}_1, \ldots, \eta_n, \dot{\eta}_n]^\top$, $n \in \mathbb{N}^+$ as [7]

$$\dot{V} = \frac{T\cos\alpha - D}{m} - g\sin\gamma, \quad \dot{h} = V\sin\gamma,$$

$$\dot{\gamma} = \frac{L + T\sin\alpha}{mV} - \frac{g\cos\gamma}{V}, \quad \dot{\alpha} = Q - \dot{\gamma},$$

$$\dot{Q} = \frac{M}{I_{yy}}, \quad \ddot{\eta}_i = -2\zeta_i\omega_i\dot{\eta}_i - \omega_i^2\eta_i + N_i, \quad i \in \mathbb{N}_{1:n}, \tag{1}$$

where $i \in \mathbb{N}_{1:n}$ denotes $i = 1, 2, \ldots, n$, rigid-body states V, h, γ, α, and Q denote velocity, altitude, FPA, AOA, and pitch rate, flexible state η_i represents amplitude of the i-th bending mode, which is obtained by modeling the fuselage as a single flexible structure with mass-normalized mode shape. m, I_{yy}, g, ζ_i, and ω_i are vehicle mass, moment of inertia, gravitational acceleration, damping ratio, and flexible mode frequency. L, D, T, M, and N_i represent lift, drag, thrust, pitching moment, and generalized elastic force. The approximations of these forces and moment are given as

$$L \approx \bar{q}SC_L(\alpha, \delta_e, \delta_c, \boldsymbol{\eta}), \quad M \approx z_T T + \bar{q}S\bar{c}C_M(\alpha, \delta_e, \delta_c, \boldsymbol{\eta}),$$

$$D \approx \bar{q}SC_D(\alpha, \delta_e, \delta_c, \boldsymbol{\eta}), \quad T \approx \bar{q}S[C_{T,\Phi}(\alpha)\Phi + C_T(\alpha) + \boldsymbol{C}_T^{\boldsymbol{\eta}}\boldsymbol{\eta}],$$

$$N_i \approx \bar{q}S[N_i^{\alpha^2}\alpha^2 + N_i^\alpha\alpha + N_i^{\delta_e}\delta_e + N_i^{\delta_c}\delta_c + N_i^0 + \boldsymbol{N}_i^{\boldsymbol{\eta}}\boldsymbol{\eta}], \quad i \in \mathbb{N}_{1:n}, \tag{2}$$

where $\bar{q}$, S, z_T, and $\bar{c}$ are dynamic press, reference area, thrust moment arm, and reference length. Φ, δ_e, and δ_c represent fuel equivalence ratio, deflection of elevator, and deflection of canard, which are the control inputs of the HFVs dynamics. The curve-fitted approximation coefficients are expressed as

$$C_D = C_D^{\alpha^2}\alpha^2 + C_D^\alpha\alpha + C_D^{\delta_e^2}\delta_e^2 + C_D^{\delta_e}\delta_e + C_D^{\delta_c^2}\delta_c^2 + C_D^{\delta_c}\delta_c + C_D^0 + \boldsymbol{C}_D^{\boldsymbol{\eta}}\boldsymbol{\eta},$$

$$C_M = C_M^{\alpha^2}\alpha^2 + C_M^\alpha\alpha + C_M^{\delta_e}\delta_e + C_M^{\delta_c}\delta_c + C_M^0 + \boldsymbol{C}_M^{\boldsymbol{\eta}}\boldsymbol{\eta},$$

$$C_L = C_L^\alpha\alpha + C_L^{\delta_e}\delta_e + C_L^{\delta_c}\delta_c + C_L^0 + \boldsymbol{C}_L^{\boldsymbol{\eta}}\boldsymbol{\eta},$$

$$C_{T,\Phi} = C_{T,\Phi}^{\alpha^3}\alpha^3 + C_{T,\Phi}^{\alpha^2}\alpha^2 + C_{T,\Phi}^\alpha\alpha + C_{T,\Phi}^0,$$

$$C_T = C_T^{\alpha^3}\alpha^3 + C_T^{\alpha^2}\alpha^2 + C_T^\alpha\alpha + C_T^0,$$

$$\boldsymbol{C}_j^{\boldsymbol{\eta}} = [C_j^{\eta_1}, 0, \ldots, C_j^{\eta_n}, 0], \quad j \in \{T, M, L, D\},$$

$$\boldsymbol{N}_i^{\boldsymbol{\eta}} = [N_i^{\eta_1}, 0, \ldots, N_i^{\eta_n}, 0], \quad i \in \mathbb{N}_{1:n}. \tag{3}$$
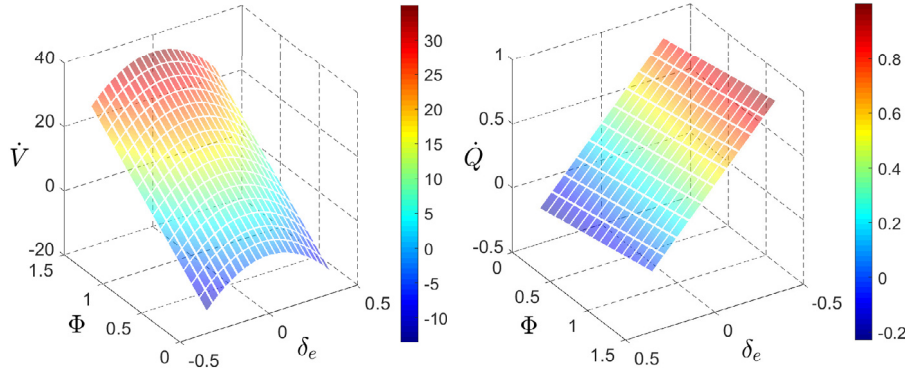
Fig. 1. The responses of $\dot{V}$ and $\dot{Q}$ along with the varying of Φ and δ_e. (For interpretation of the colors in the figures, the reader is referred to the web version of this article.)

Herein, to cancel the lift-elevator coupling, δ_c is set to be ganged with δ_e, i.e., $\delta_c = k_{e,c}\delta_e$ with $k_{e,c} = -C_L^{\delta_e}/C_L^{\delta_c}$. As such, the control inputs of HFVs become Φ and δ_e. According to the strict requirements in terms of working conditions of HFVs, the states in (1) must operate in constrained regions that are not symmetric. To make an example, a typical operating region characterizing hypersonic flight and operability of scramjet engines can be the hypercube [4]

$$\Omega_0 \triangleq \Big\{ 85000 \le h \le 135000[\text{ft}], \, 7500 \le V \le 11500[\text{ft/s}],$$

$$-5 \le \gamma \le 7[\text{deg}], \, -5 \le \alpha \le 10[\text{deg}], \, -10 \le Q \le 10[\text{deg/s}] \Big\}.$$

Hereafter, we will deal with such an asymmetric region via the time-varying asymmetric thresholds $-k_{x,L}(t)$ (lower threshold) and $k_{x,H}(t)$ (upper threshold) for the corresponding state tracking error $s_x(t)$, $x \in \Omega_x \triangleq \{h, \gamma, \alpha, Q, V\}$ [32–37]. For safety and reliability reasons, the reference trajectories V_r and h_r are restricted to a subset $\Omega_r \subset \Omega_0$. The control objective of this study is to design the fixed-time command-filtered trajectory tracking control methodology such that: 1) the tracking errors of velocity and altitude converge into the user-defined residual sets within fixed time; 2) all flight state variables of the resulting closed-loop system remain bounded; and 3) the asymmetric envelope constraints are never violated.

2.2. Model decomposition

As shown in Fig. 1, Φ and δ_e appear to vary linearly and have a more significant effect on $\dot{V}$ and $\dot{Q}$ respectively, inspiring us to decompose the longitudinal HFVs model (1) into the following velocity and altitude dynamics [12,13]. Considering that aerodynamic coefficients and atmospheric parameters constantly change from earth to near space, the uncertain velocity dynamics is formulated from (1)-(3) as [15,16]

$$\dot{V} = \boldsymbol{\zeta}_V^\top (\boldsymbol{f}_V + \boldsymbol{g}_V \Phi) + d_V, \tag{4}$$

where

$$\boldsymbol{f}_V = \bar{q} \big[\mathbf{0}^{1\times4}, \alpha^3\cos\alpha, \alpha^2\cos\alpha, \alpha\cos\alpha, \cos\alpha, -\alpha^2, -\alpha, -\delta_e^2, -\delta_e, -1, -\frac{g}{\bar{q}}\sin\gamma \big]^\top$$

$$\boldsymbol{\zeta}_V = \frac{S}{m} \big[C_{T,\Phi}^{\alpha^3}, C_{T,\Phi}^{\alpha^2}, C_{T,\Phi}^{\alpha}, C_{T,\Phi}^0, C_T^{\alpha^3}, C_T^{\alpha^2}, C_T^{\alpha}, C_T^0, C_D^{\alpha^2}, C_D^{\alpha}, (C_D^{\delta_e^2} + k_{e,c}^2 C_D^{\delta_c^2}),$$

$$(C_D^{\delta_e} + k_{e,c} C_D^{\delta_c}), C_D^0, \frac{m}{S} \big]^\top, \quad \boldsymbol{g}_V = \bar{q}\cos\alpha \big[\alpha^3, \alpha^2, \alpha, 1, \mathbf{0}^{1\times10} \big]^\top,$$

and the lumped disturbances d_V, brought by external disturbances such as gust, turbulence, and atmospheric disturbances, as well as structural flexibility from the aerothermoelastic effects, can be expressed as $d_V = \frac{\bar{q}S}{m}\boldsymbol{C}_T^\eta \boldsymbol{\eta}\cos\alpha - \frac{\bar{q}S}{m}\boldsymbol{C}_D^\eta \boldsymbol{\eta} + \Delta_V$, with Δ_V representing the external disturbances.

From the viewpoint of engineering, FPA γ is quite small during the cruise phase, thus we take $\sin\gamma \approx \gamma$ for simplicity [33]. In addition, AOA α is small enough such that the term $T\sin\alpha$ is far smaller than lift L, thus $T\sin\alpha$ can be neglected in (1) [30]. Therefore, the altitude dynamics can be transformed as [15,16]

$$\begin{cases} \dot{h} = V\gamma + d_h, \\ \dot{\gamma} = \boldsymbol{\zeta}_\gamma^\top (\boldsymbol{f}_\gamma + \boldsymbol{g}_\gamma \alpha) + d_\gamma, \\ \dot{\alpha} = \boldsymbol{\zeta}_\alpha^\top (\boldsymbol{f}_\alpha + \boldsymbol{g}_\alpha Q) + d_\alpha, \\ \dot{Q} = \boldsymbol{\zeta}_Q^\top (\boldsymbol{f}_Q + \boldsymbol{g}_Q \delta_e) + d_Q, \end{cases} \tag{5}$$

where

$$\boldsymbol{f}_\gamma = [0, \frac{\bar{q}}{V}, -\frac{g}{V}\cos\gamma]^\top, \boldsymbol{f}_\alpha = \frac{\bar{q}}{V}[0, -\alpha, -1, \frac{g}{\bar{q}}\cos\gamma]^\top, \boldsymbol{f}_Q = \bar{q}[\boldsymbol{0}^{1\times2}, \alpha^3\Phi, \alpha^2\Phi,$$

$$\alpha\Phi, \Phi, \alpha^3, \alpha^2, \alpha, 1]^\top, \boldsymbol{\zeta}_\gamma = [\frac{S}{m}C_L^\alpha, \frac{S}{m}C_L^0, 1]^\top, \boldsymbol{\zeta}_\alpha = [1, \frac{S}{m}C_L^\alpha, \frac{S}{m}C_L^0, 1]^\top,$$

$$\boldsymbol{\zeta}_Q = \frac{S}{I_{yy}}[\bar{c}C_M^{\delta_e}, \bar{c}k_{e,c}C_M^{\delta_c}, z_T C_{T,\Phi}^{\alpha^3}, z_T C_{T,\Phi}^{\alpha^2}, z_T C_{T,\Phi}^\alpha, z_T C_{T,\Phi}^0, z_T C_T^{\alpha^3}, (z_T C_T^{\alpha^2}$$

$$+ \bar{c}C_M^{\alpha^2}), (z_T C_T^\alpha + \bar{c}C_M^\alpha), (z_T C_T^0 + \bar{c}C_M^0)]^\top, \boldsymbol{g}_\gamma = [\frac{\bar{q}}{V}, \boldsymbol{0}^{1\times2}]^\top,$$

$$\boldsymbol{g}_\alpha = [1, \boldsymbol{0}^{1\times3}]^\top, \boldsymbol{g}_Q = [\bar{q}, \bar{q}, \boldsymbol{0}^{1\times8}]^\top,$$

and the lumped disturbances $d_h = \Delta_h$, $d_\gamma = \frac{\bar{q}S}{mV}\boldsymbol{C}_L^\eta\boldsymbol{\eta} + \Delta_\gamma$, $d_\alpha = -\frac{\bar{q}S}{mV}\boldsymbol{C}_L^\eta\boldsymbol{\eta} + \Delta_\alpha$, and $d_Q = \frac{z_T\bar{q}S}{I_{yy}}\boldsymbol{C}_T^\eta\boldsymbol{\eta} + \frac{\bar{q}S\bar{c}}{I_{yy}}\boldsymbol{C}_M^\eta\boldsymbol{\eta} + \Delta_Q$, with Δ_h, Δ_γ, Δ_α, and Δ_Q representing the external disturbances.

2.3. Actuator fault modeling

Typically, there are two pieces of elevators installed on a HFV, i.e., the right one and left one [13]. Without loss of generality, the overall elevator deflection δ_e is modeled as a linear combination $\delta_e = \varsigma_{e,1}\delta_{e,1} + \varsigma_{e,2}\delta_{e,2}$, where $\varsigma_{e,i}$ and $\delta_{e,i}$ $(i \in \mathbb{N}_{1:2})$ are elevator gain and deflection, respectively.

In aerospace engineering, the leakage of hydraulic fluid may lead to the degradation of the actuator effectiveness. Moreover, the sensor fault and elevator hysteresis shall cause the bias. By considering loss of effectiveness and bias simultaneously, the elevator fault model can be described as

$$\delta_{e,i}(t) = \sigma_{i,p}\delta_{i,\mathrm{cmd}}(t) + \upsilon_{i,p}, \quad i \in \mathbb{N}_{1:2}, \quad t \in [t_{ip,b}, t_{ip,e}), \tag{6}$$

where $\delta_{i,\mathrm{cmd}}$ represents the desired control command for the i-th elevator, $\sigma_{i,p} \in [0, 1]$ is the actuator effectiveness factor, $p \in \mathbb{N}^+$ denotes the p-th fault model, $\upsilon_{i,p}$ is the bounded bias, $t_{ip,b}$ and $t_{ip,e}$ denote the time instants when the p-th fault takes place and ends on the i-th elevator.

Remark 1. Notice that (6) implies the following three cases:

- $\sigma_{i,p} = 1$ and $\upsilon_{i,p} = 0$. This indicates the fault-free case.
- $0 < \underline{\sigma}_{i,p} \le \sigma_{i,p} \le \overline{\sigma}_{i,p} < 1$ and $\upsilon_{i,p} = 0$, with $\underline{\sigma}_{i,p}$ and $\overline{\sigma}_{i,p}$ being unknown positive constants. This case corresponds to the partial loss of effectiveness (PLOE).
- $\sigma_{i,p} = 0$ and $\upsilon_{i,p} \ne 0$. This fact is known as the total loss of effectiveness (TLOE) that $\delta_{e,i}$ is stuck at an unknown value $\upsilon_{i,p}$. For the controllability, only up to one elevator is allowed to undergo TLOE at the same time.

Similar to (6), we consider the actual fuel equivalence ratio subject to loss of effectiveness and bias described by [13]

$$\Phi(t) = \sigma_{V,p}\Phi_{\mathrm{cmd}}(t) + \upsilon_{V,p}, \quad t \in [t_{Vp,b}, t_{Vp,e}), \tag{7}$$

where $\sigma_{V,p} \in [0, 1]$ is the actuator effectiveness factor, $p \in \mathbb{N}^+$ denotes the p-th fault model, $\upsilon_{V,p}$ is the bounded bias, $t_{Vp,b}$ and $t_{Vp,e}$ denote the time instants when the p-th fault takes place and ends.

2.4. Technical key lemmas

The following technical lemmas will be employed to derive the main results of this paper.

Lemma 1. *For a generic dynamical system $\dot{x}(t) = f(t, x)$, $f(t, 0) = 0$, $x(0) = x_0$, where $x \in \Omega_x \subset \mathbb{R}^n$, $f : \mathbb{R}^+ \times \Omega_x \to \mathbb{R}^n$, and origin is an equilibrium point, if $\Omega_x = \mathbb{R}^n$ and there exists a Lyapunov function $\mathcal{L}(x)$ defined on $\mathbb{R}^n$ satisfying*

$$\dot{\mathcal{L}}(x) \le -(\alpha\mathcal{L}^p(x) + \beta\mathcal{L}^q(x))^\kappa,$$

where α, β, p, q, and κ are some positive constants, $p\kappa > 1$ and $q\kappa < 1$, then the origin of the system is fixed-time stable, and the settling time satisfies $T(x_0) \le \frac{1}{\alpha^\kappa(p\kappa-1)} + \frac{1}{\beta^\kappa(1-q\kappa)}$ for a given initial condition $x_0 \in \mathbb{R}^n$ [31].
To be specific, if $\kappa = 1$ and there exists a Lyapunov function $\mathcal{L}(x)$ defined on $\Omega_{x,0} \subseteq \Omega_x \subset \mathbb{R}^n$ satisfying

$$\dot{\mathcal{L}}(x) \le -\alpha\mathcal{L}^p(x) - \beta\mathcal{L}^q(x),$$

where α, β, $p > 1$, and $q < 1$ are some positive constants, then the origin of the system is locally fixed-time stable, and the settling time satisfies $T(x_0) \le \frac{1}{\alpha(p-1)} + \frac{1}{\beta(1-q)}$ for a given initial condition $x_0 \in \Omega_{x,0}$.

Lemma 2. *For any given positive constants c_0, c_1, and c_2, the following inequality holds [38–40]*

$$|\xi|^{c_0}|\zeta|^{c_1} \le \frac{c_0 c_2}{c_1 + c_2}|\xi|^{c_0+c_1} + \frac{c_1}{c_1 + c_2}c_2^{-\frac{c_0}{c_1}}|\zeta|^{c_0+c_1},$$

where ξ and ζ are any real variables.

3. Fixed-time command-filtered control design

To start the design, let us introduce the tracking errors $z_V = V - V_r$, $z_h = h - h_r$, $z_\gamma = \gamma - \gamma_d$, $z_\alpha = \alpha - \alpha_d$, and $z_Q = Q - Q_d$, where γ_d, α_d, Q_d and their derivatives $\dot{\gamma}_d$, $\dot{\alpha}_d$, $\dot{Q}_d$ are generated by filtering the virtual control laws γ_{cmd}, α_{cmd}, Q_{cmd} via the following fixed-time command filter [41]:

$$\begin{cases} \dot{\widehat{x}}_1 = \widehat{x}_2 - \tau_1 \lfloor \widehat{x}_1 - x_r \rceil^{p_1} - \iota_1 \lfloor \widehat{x}_1 - x_r \rceil^{q_1}, \\ \dot{\widehat{x}}_2 = -\tau_2 \lfloor \widehat{x}_1 - x_r \rceil^{p_2} - \iota_2 \lfloor \widehat{x}_1 - x_r \rceil^{q_2}, \end{cases} \tag{8}$$

where x_r is the input signal, $\lfloor \cdot \rceil^l$ denotes $|\cdot|^l \mathrm{sgn}(\cdot)$, positive design parameters $p_1 \in (1, 1 + \varepsilon_p)$, $q_1 \in (1 - \varepsilon_q, 1)$, $p_2 = 2p_1 - 1$, $q_2 = 2q_1 - 1$, with ε_p and ε_q being sufficiently small positive constants. Furthermore, the filter gains τ_i and ι_i ($i \in \mathbb{N}_{1:2}$) are assigned such that the matrices

$$\boldsymbol{\Gamma}_1 = \begin{bmatrix} -\tau_1 & 1 \\ -\tau_2 & 0 \end{bmatrix}, \quad \boldsymbol{\Gamma}_2 = \begin{bmatrix} -\iota_1 & 1 \\ -\iota_2 & 0 \end{bmatrix},$$

are Hurwitz, then the following lemma holds.

Lemma 3. *For the fixed-time command filter (8), the filter state $\widehat{x}_1$ can converge to the input signal x_r in a fixed time:*

$$\mathcal{T}_1 \leq \mathcal{T}_{1,\max} \triangleq \frac{\lambda_{\max}^{2-q_1}(\boldsymbol{P}_2)}{(1-q_1)\lambda_{\min}(\boldsymbol{Q}_2)} + \frac{\lambda_{\max}(\boldsymbol{P}_1)}{(p_1-1)\xi^{p_1-1}\lambda_{\min}(\boldsymbol{Q}_1)},$$

where $\lambda_{\min}(\boldsymbol{A})$ and $\lambda_{\max}(\boldsymbol{A})$ are the minimum and maximum eigenvalues of the matrix $\boldsymbol{A}$, $\xi \leq \lambda_{\min}(\boldsymbol{P}_1)$ is a positive constant, $\boldsymbol{P}_1$, $\boldsymbol{P}_2$, $\boldsymbol{Q}_1$, and $\boldsymbol{Q}_2$ are the symmetric positive-definite matrices satisfying

$$\boldsymbol{P}_1 \boldsymbol{\Gamma}_1 + \boldsymbol{\Gamma}_1 \boldsymbol{P}_1 = -\boldsymbol{Q}_1, \quad \boldsymbol{P}_2 \boldsymbol{\Gamma}_2 + \boldsymbol{\Gamma}_2 \boldsymbol{P}_2 = -\boldsymbol{Q}_2,$$

where the matrices $\boldsymbol{\Gamma}_1$ and $\boldsymbol{\Gamma}_2$ are defined after (8).

Proof. The detailed proof for Lemma 3 can be found in Theorem 3 of [41], thus is omitted here for space limitations. $\square$

Subsequently, along the command-filtered backstepping design [23–27], let us define the compensated error $s_V = z_V$, $s_h = z_h - \chi_\gamma$, $s_\gamma = z_\gamma - \chi_\alpha$, $s_\alpha = z_\alpha - \chi_Q$, and $s_Q = z_Q$, and the compensated signals χ_γ, χ_α, and χ_Q as

$$\begin{cases} \dot{\chi}_\gamma = -c_{\gamma,1}\chi_\gamma - c_{\gamma,2}\chi_\gamma^3 - \ell_\gamma \mathrm{sgn}(\chi_\gamma) + V(\gamma_d - \gamma_{\mathrm{cmd}} + \chi_\alpha), \\ \dot{\chi}_\alpha = -c_{\alpha,1}\chi_\alpha - c_{\alpha,2}\chi_\alpha^3 - \ell_\alpha \mathrm{sgn}(\chi_\alpha) + \boldsymbol{\zeta}_\gamma^\top \boldsymbol{g}_\gamma(\alpha_d - \alpha_{\mathrm{cmd}} + \chi_Q), \\ \dot{\chi}_Q = -c_{Q,1}\chi_Q - c_{Q,2}\chi_Q^3 - \ell_Q \mathrm{sgn}(\chi_Q) + \boldsymbol{\zeta}_\alpha^\top \boldsymbol{g}_\alpha(Q_d - Q_{\mathrm{cmd}}), \end{cases} \tag{9}$$

where $c_{z,1}$, $c_{z,2}$, and ℓ_z are positive design parameters for $z \in \Omega_z \triangleq \{\gamma, \alpha, Q\}$.

Before moving on, utilizing the error coordinate s_x ($x \in \Omega_x$), a time-varying asymmetric BLF is devised as

$$\mathcal{L}_{\mathcal{Z}_x} = \frac{1}{2} \mathcal{Z}_x^2, \quad \mathcal{Z}_x = \frac{k_{x,H} k_{x,L} s_x}{(k_{x,H} - s_x)(k_{x,L} + s_x)}. \tag{10}$$

Calculating the time derivative of $\mathcal{L}_{\mathcal{Z}_x}$ along (10) yields

$$\dot{\mathcal{L}}_{\mathcal{Z}_x} = \mathcal{Z}_x \left(\frac{\partial \mathcal{Z}_x}{\partial k_{x,H}} \dot{k}_{x,H} + \frac{\partial \mathcal{Z}_x}{\partial k_{x,L}} \dot{k}_{x,L} + \frac{\partial \mathcal{Z}_x}{\partial s_x} \dot{s}_x \right) = \mathcal{Z}_x \varphi_x \dot{s}_x + \mathcal{Z}_x \varsigma_x, \tag{11}$$

where

$$\varsigma_x = \frac{k_{x,H} \dot{k}_{x,L} s_x^2}{(k_{x,H} - s_x)(k_{x,L} + s_x)^2} - \frac{k_{x,L} \dot{k}_{x,H} s_x^2}{(k_{x,H} - s_x)^2(k_{x,L} + s_x)},$$

$$\varphi_x = \frac{k_{x,H} k_{x,L}(s_x^2 + k_{x,H} k_{x,L})}{(k_{x,H} - s_x)^2(k_{x,L} + s_x)^2} > 0.$$

To further facilitate the control design and stability analysis, let us define the following variables:

$$\begin{cases} \phi_{\delta_e} = \sup_{t \geq 0} \sum_{i=1}^{2} \left| \boldsymbol{\zeta}_Q^\top \boldsymbol{g}_Q \varsigma_{e,i} \upsilon_{i,p} \right|, \quad \omega_{\delta_e} = \inf_{t \geq 0} \sum_{i=1}^{2} \varsigma_{e,i} \sigma_{i,p}, \quad \xi_{\delta_e} = \frac{1}{\omega_{\delta_e}}, \\ \phi_\Phi = \sup_{t \geq 0} \left\{ \left| \boldsymbol{\zeta}_V^\top \boldsymbol{g}_V \upsilon_{V,p} \right| \right\}, \quad \omega_\Phi = \inf_{t \geq 0} \{\sigma_{V,p}\}, \quad \xi_\Phi = \frac{1}{\omega_\Phi}, \end{cases} \tag{12}$$

and $\vartheta_V = d_V^* + \phi_\Phi$, $\vartheta_h = d_h^* + \ell_\gamma$, $\vartheta_\gamma = d_\gamma^* + \ell_\alpha$, $\vartheta_\alpha = d_\alpha^* + \ell_Q$, $\vartheta_Q = d_Q^* + \phi_{\delta_e}$, where constant d_x^* satisfies $d_x^* \geq |d_x|$.

Table 1
The control laws and adaptation laws.

Control laws

$$\gamma_{\mathrm{cmd}} = -\frac{\gamma_c \,\mathrm{sg}(\mathscr{Z}_h \gamma_c | \varepsilon)}{\varphi_h V}, \qquad \alpha_{\mathrm{cmd}} = -\frac{\alpha_c \,\mathrm{sg}(\mathscr{Z}_\gamma \alpha_c | \varepsilon)}{\varphi_\gamma \boldsymbol{\zeta}_\gamma^\top \boldsymbol{g}_\gamma},$$

$$Q_{\mathrm{cmd}} = -\frac{Q_c \,\mathrm{sg}(\mathscr{Z}_\alpha Q_c | \varepsilon)}{\varphi_\alpha \boldsymbol{\zeta}_\alpha^\top \boldsymbol{g}_\alpha}, \ \ \delta_{i,\mathrm{cmd}} = -\frac{\widehat{\xi}_{\delta_e} \delta_c \,\mathrm{sg}(\mathscr{Z}_Q \widehat{\xi}_{\delta_e} \delta_c | \varepsilon)}{\varphi_Q \boldsymbol{\zeta}_Q^\top \boldsymbol{g}_Q},$$

$$\Phi_{\mathrm{cmd}} = -\frac{\widehat{\xi}_\Phi \Phi_c \,\mathrm{sg}(\mathscr{Z}_V \widehat{\xi}_\Phi \Phi_c | \varepsilon)}{\varphi_V \boldsymbol{\zeta}_V^\top \boldsymbol{g}_V}, \tag{13}$$

with

$$\gamma_c = \kappa_{h,1} \mathscr{Z}_h^p + \kappa_{h,2} \psi(\mathscr{Z}_h) + c_{\gamma,1} \varphi_h \chi_\gamma + c_{\gamma,2} \varphi_h \chi_\gamma^3 - \varphi_h \dot{h}_r$$
$$\qquad + \widehat{\vartheta}_h \varphi_h \,\mathrm{sg}(\mathscr{Z}_h \varphi_h | \varepsilon) + \varsigma_h,$$

$$\alpha_c = \kappa_{\gamma,1} \mathscr{Z}_\gamma^p + \kappa_{\gamma,2} \psi(\mathscr{Z}_\gamma) + c_{\alpha,1} \varphi_\gamma \chi_\alpha + c_{\alpha,2} \varphi_\gamma \chi_\alpha^3 - \varphi_\gamma \dot{\gamma}_d$$
$$\qquad + \widehat{\vartheta}_\gamma \varphi_\gamma \,\mathrm{sg}(\mathscr{Z}_\gamma \varphi_\gamma | \varepsilon) + \varphi_\gamma \boldsymbol{\zeta}_\gamma^\top \boldsymbol{f}_\gamma + \mathscr{Z}_h \varphi_h V \beta_\gamma + \varsigma_\gamma,$$

$$Q_c = \kappa_{\alpha,1} \mathscr{Z}_\alpha^p + \kappa_{\alpha,2} \psi(\mathscr{Z}_\alpha) + c_{Q,1} \varphi_\alpha \chi_Q + c_{Q,2} \varphi_\alpha \chi_Q^3 - \varphi_\alpha \dot{\alpha}_d$$
$$\qquad + \widehat{\vartheta}_\alpha \varphi_\alpha \,\mathrm{sg}(\mathscr{Z}_\alpha \varphi_\alpha | \varepsilon) + \varphi_\alpha \boldsymbol{\zeta}_\alpha^\top \boldsymbol{f}_\alpha + \mathscr{Z}_\gamma \varphi_\gamma \boldsymbol{\zeta}_\gamma^\top \boldsymbol{g}_\gamma \beta_\alpha + \varsigma_\alpha,$$

$$\delta_c = \kappa_{Q,1} \mathscr{Z}_Q^p + \kappa_{Q,2} \psi(\mathscr{Z}_Q) + \varphi_Q \boldsymbol{\zeta}_Q^\top \boldsymbol{f}_Q - \varphi_Q \dot{Q}_d + \varsigma_Q$$
$$\qquad + \widehat{\vartheta}_Q \varphi_Q \,\mathrm{sg}(\mathscr{Z}_Q \varphi_Q | \varepsilon) + \mathscr{Z}_\alpha \varphi_\alpha \boldsymbol{\zeta}_\alpha^\top \boldsymbol{g}_\alpha \beta_Q,$$

$$\Phi_c = \kappa_{V,1} \mathscr{Z}_V^p + \kappa_{V,2} \psi(\mathscr{Z}_V) + \varphi_V \boldsymbol{\zeta}_V^\top \boldsymbol{f}_V - \varphi_V \dot{V}_r + \varsigma_V$$
$$\qquad + \widehat{\vartheta}_V \varphi_V \,\mathrm{sg}(\mathscr{Z}_V \varphi_V | \varepsilon).$$

Adaptation laws

$$\dot{\widehat{\xi}}_{\delta_e} = \rho_{\delta_e} \mathscr{Z}_Q \delta_c - \rho_{\delta_e} \sigma_{\delta_e} \widehat{\xi}_{\delta_e}, \ \ \dot{\widehat{\xi}}_\Phi = \rho_\Phi \mathscr{Z}_V \Phi_c - \rho_\Phi \sigma_\Phi \widehat{\xi}_\Phi,$$

$$\dot{\widehat{\vartheta}}_h = \rho_h \mathscr{Z}_h \varphi_h \,\mathrm{sg}(\mathscr{Z}_h \varphi_h | \varepsilon) - \rho_h \sigma_h \widehat{\vartheta}_h,$$

$$\dot{\widehat{\vartheta}}_\gamma = \rho_\gamma \mathscr{Z}_\gamma \varphi_\gamma \,\mathrm{sg}(\mathscr{Z}_\gamma \varphi_\gamma | \varepsilon) - \rho_\gamma \sigma_\gamma \widehat{\vartheta}_\gamma,$$

$$\dot{\widehat{\vartheta}}_\alpha = \rho_\alpha \mathscr{Z}_\alpha \varphi_\alpha \,\mathrm{sg}(\mathscr{Z}_\alpha \varphi_\alpha | \varepsilon) - \rho_\alpha \sigma_\alpha \widehat{\vartheta}_\alpha,$$

$$\dot{\widehat{\vartheta}}_Q = \rho_Q \mathscr{Z}_Q \varphi_Q \,\mathrm{sg}(\mathscr{Z}_Q \varphi_Q | \varepsilon) - \rho_Q \sigma_Q \widehat{\vartheta}_Q,$$

$$\dot{\widehat{\vartheta}}_V = \rho_V \mathscr{Z}_V \varphi_V \,\mathrm{sg}(\mathscr{Z}_V \varphi_V | \varepsilon) - \rho_V \sigma_V \widehat{\vartheta}_V. \tag{14}$$

At this stage, let us devise the control laws and adaptation laws as summarized in Table 1 (13)-(14), where $\kappa_{x,1}$, $\kappa_{x,2}$, σ_x, σ_u, $\rho_x = \frac{2c_x}{2c_x-1}$, $\rho_u = \frac{2c_u}{2c_u-1}$, and ε are positive design parameters with $c_x > \frac{1}{2}$, $c_u > \frac{1}{2}$, and $u \in \Omega_u \triangleq \{\Phi, \delta_e\}$, $p = p_1/p_2 > 1$, $q = q_1/q_2 < 1$ with positive odd integers p_1, p_2, q_1, and q_2, $\mathrm{sg}(x | \varepsilon) = \frac{x}{\sqrt{x^2+\varepsilon^2}}$, $\beta_x = \frac{(k_{x,H}-s_x)(k_{x,L}+s_x)}{k_{x,H} k_{x,L}}$, and switching function

$$\psi(\mathscr{Z}_x) = \boldsymbol{S}^\top(\mathscr{Z}_x) \boldsymbol{\Upsilon}(\mathscr{Z}_x), \tag{15}$$

with

$$\boldsymbol{S}(\mathscr{Z}_x) = \begin{cases} [1, 0]^\top, & \text{if } |\mathscr{Z}_x| \geq \nu_x, \\ [0, 1]^\top, & \text{otherwise}, \end{cases}$$

and $\boldsymbol{\Upsilon}(\mathscr{Z}_x) = \left[\mathscr{Z}_x^q, \sum_{i=1}^{2n-1} l_i \mathscr{Z}_x^i \nu_x^{q-i}\right]^\top$ for positive constants ν_x and l_i $(i = 1, 3, \ldots, 2n-1, n \in \mathbb{N}^+)$ determined by

$$\begin{bmatrix} k_1 \\ k_3 \\ k_5 \\ \vdots \\ k_{2n-1} \end{bmatrix} = \begin{bmatrix} 1 & 1 & \cdots & 1 \\ 1 & 3 & \cdots & 2n-1 \\ 0 & 3 \times 2 & \cdots & (2n-1)(2n-2) \\ \vdots & \vdots & \ddots & \vdots \\ 0 & 0 & \ldots & \prod_{i=1}^{n-1}(2n-i) \end{bmatrix} \begin{bmatrix} l_1 \\ l_3 \\ l_5 \\ \vdots \\ l_{2n-1} \end{bmatrix},$$

where $k_1 = 1$, $k_3 = q$, $k_5 = q(q-1)$, $\ldots$, and $k_{2n-1} = \prod_{i=1}^{n-1}(q-i+1)$. Up to now, the fixed-time command-filtered control design has been completed, whose architecture is sketched in Fig. 2.
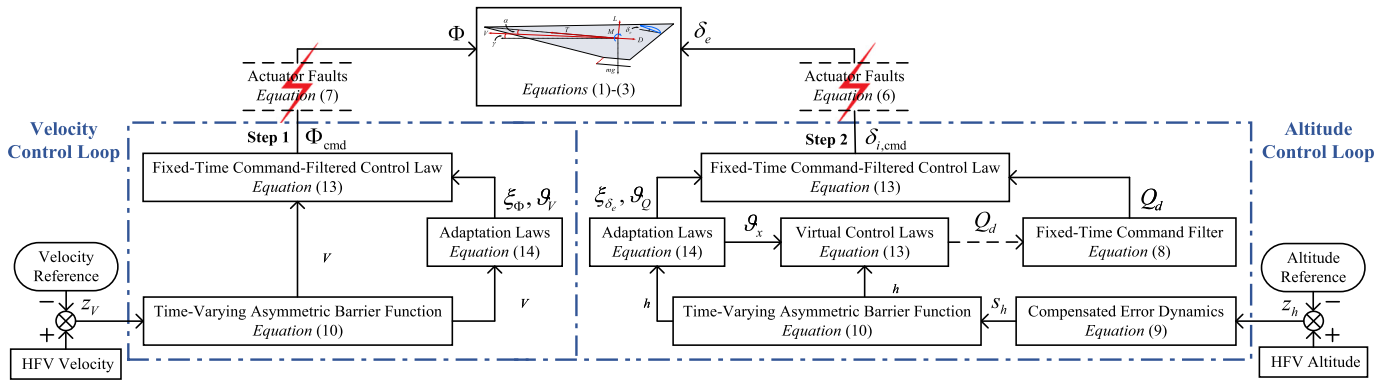
Fig. 2. The overall control architecture of the proposed method.

Table 2
Proof sketch for Theorem 1.

Proof sketch	
Step 1.	Calculate $\dot{\mathcal{L}}_{\mathcal{Z}_V}$ for velocity dynamics.
Step 2.	Calculate $\dot{\mathcal{L}}_{\mathcal{Z}_h}$, $\dot{\mathcal{L}}_{\mathcal{Z}_\gamma}$, $\dot{\mathcal{L}}_{\mathcal{Z}_\alpha}$, and $\dot{\mathcal{L}}_{\mathcal{Z}_Q}$ for altitude dynamics.
Step 3.	Calculate $\dot{\mathcal{L}}_\vartheta$ and $\dot{\mathcal{L}}_\xi$, and accumulate the results of Steps 1-2, verify that all the signals in the closed-loop system are bounded.
Step 4.	Analyze the convergence rate and region of χ_γ, χ_α, χ_Q, z_h, and z_V.

Remark 2. The switching function $\psi(\mathcal{Z}_x)$ in (15) is devised to fulfill the requirement for numerical differentiation in input signal of command filter. In the controller design procedure of existing relevant literature (see [26–31] and the references therein), the feedback term $\psi(\mathcal{Z}_x) = \mathcal{Z}_x^q$ guarantees the desired finite-time convergence, where $0 < q < 1$ for $\forall \mathcal{Z}_x \in \mathbb{R}$. However, this choice might result in a singularity issue (non-differentiability), i.e., $\dot{\psi}(\mathcal{Z}_x) = q\mathcal{Z}_x^{q-1} \to \infty$ as $\mathcal{Z}_x \to 0$. As a result, the command-filtered backstepping approach cannot be applied directly. To overcome this singularity, the switching function $\psi(\mathcal{Z}_x)$ in (15) is skillfully designed to be continuous and differentiable, which further ensures the absence of the singularity issue in our work.

4. Stability analysis

In this section, the stability analysis for the whole HFVs dynamics will be presented. Initially, let us construct the following overall Lyapunov function:

$$\mathcal{L} = \mathcal{L}_{\mathcal{Z}} + \mathcal{L}_\vartheta + \mathcal{L}_\xi, \tag{16}$$

where $\mathcal{L}_\vartheta = \sum_{i \in \Omega_x} \frac{1}{2\rho_i} \widetilde{\vartheta}_i^2$, $\mathcal{L}_\xi = \sum_{j \in \Omega_u} \frac{1}{2\rho_j} \omega_j \widetilde{\xi}_j^2$, and $\mathcal{L}_{\mathcal{Z}} = \sum_{i \in \Omega_x} \mathcal{L}_{\mathcal{Z}_i}$ with $\mathcal{L}_{\mathcal{Z}_i}$ being the time-varying asymmetric BLF specified in (10). Then, the main results of our work are now given as follows.

Theorem 1. *Consider the velocity dynamics (4) and altitude dynamics (5) in the presence of diverse actuator faults and asymmetric envelope constraints. Under the fixed-time control laws (13) and adaptation laws (14) for any initial condition $-k_{x,L}(0) \le s_x(0) \le k_{x,H}(0)$, $x \in \Omega_x$, the following goals can be achieved: 1) V and h are driven to track the reference trajectories V_r and h_r in fixed time; 2) all the signals in velocity dynamics (4) and altitude dynamics (5) are bounded; 3) the asymmetric envelope constraints are never violated.*

Proof. See Appendix for the proof where a proof sketch is given in Table 2 to make the proof procedure more clear. The proof will be divided into four steps. We begin the proof with the investigation of the time derivative of $\mathcal{L}_{\mathcal{Z}_x}$ in Steps 1-2. In the sequel, the main results in Theorem 1 will be obtained in Steps 3-4 by fusing the analysis in Steps 1-2. □

Remark 3. It is well documented that the convergence rate of command filter is vital to the performance of whole control system, especially for the safety-critical HFVs working in the harsh flight environment. In contrast to extant command filters whose estimation errors are convergent asymptotically [23–25] or within a finite time [26,27], the resorted fixed-time command filter (8) is capable of estimating the unavailable state in fixed time irrelevant to the initial conditions, facilitating the control design and stability analysis.

5. Simulation results

This section presents the simulation tests of the proposed fixed-time asymmetric-constrained control (PFCC) in contrast to the extant results, i.e., the conventional infinite-time symmetric-constrained control (CICC) [32] and infinite-time unconstrained control (CIUC) [15]. The vehicle is assumed to climb a maneuver where the reference commands are set as an increment of 1000 ft/s step signal in velocity dynamics and an increment of 3000 ft step signal in altitude dynamics. To make the given commands more realizable, the trajectories of V_r, h_r and their derivatives are generated by filtering the reference commands via tracking differentiators [15]. According to the practical engineering characteristics, the limitations of actuators are set as $\Phi \in [0.05, 1.2]$ and $\delta_e \in [-20\,\text{deg}, 20\,\text{deg}]$. The external disturbances are described by the following second-order Markov process
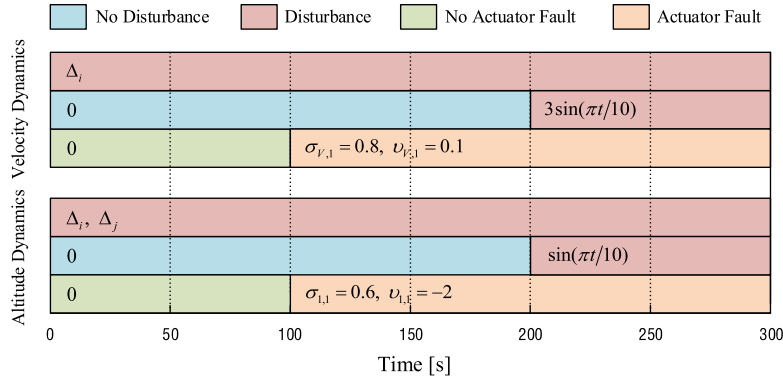
Fig. 3. Disturbances and actuator faults in the simulations.

$$\begin{cases} \ddot{\Delta}_i = -\dot{\Delta}_i - \Delta_i + 0.01\varpi_i, \\ \ddot{\Delta}_j = -\dot{\Delta}_j - \Delta_j + \varpi_j, \end{cases} \quad (17)$$

where $i \in \{h, V\}$, $j \in \{\gamma, \alpha, Q\}$, ϖ_i and ϖ_j are two independent Gauss white noises with the variance of 1. The uncertain aerodynamic coefficients in (3) are modeled as $C_i = C_i^*(1 + \sigma_i)$, where C_i^* represents the nominal coefficient and σ_i represents the uncertain factor ranging from -30% to 30%. To further verify the robustness of the proposed control methodology, the perturbations $3\sin(\frac{\pi}{10}t)$ and $\sin(\frac{\pi}{10}t)$ are added to the velocity dynamics and altitude dynamics respectively when $t > 200\,\mathrm{s}$. On the basis of (6) and (7), the fault models $\sigma_{1,1} = 0.6$, $\upsilon_{1,1} = -2$, $\sigma_{V,1} = 0.8$, and $\upsilon_{V,1} = 0.1$ are introduced when $t > 100\,\mathrm{s}$. To sum up, the actuator faults and external disturbances imposed on velocity dynamics and altitude dynamics are summarized in Fig. 3.

The parameters of control laws and adaptation laws are chosen as: $\kappa_{h,1} = 5.5$, $\kappa_{h,2} = 25$, $\kappa_{\gamma,1} = 2.5$, $\kappa_{\gamma,2} = 1$, $\kappa_{\alpha,1} = 1.2$, $\kappa_{\alpha,2} = 0.75$, $\kappa_{Q,1} = 10$, $\kappa_{Q,2} = 1.2$, $\kappa_{V,1} = 5$, $\kappa_{V,2} = 10$, $p = 5/3$, $q = 3/5$, $l_1 = 6/5$, $l_3 = -1/5$, $\varepsilon = 0.1$, $v_x = 0.05$, $c_{z,1} = 0.75$, $c_{z,2} = 1$, $\ell_z = 0.5$, $c_x = c_u = 0.6$, $\rho_x = \rho_u = 6$, and $\sigma_x = \sigma_u = 0.5$, for $x \in \Omega_x$, $z \in \Omega_z$, and $u \in \Omega_u$. The parameters of command filters are set as $\tau_1 = \iota_1 = 1$, $\tau_2 = \iota_2 = 0.25$, $p_1 = 1.1$, $p_2 = 1.2$, $q_1 = 0.9$, and $q_2 = 0.8$. The time-varying asymmetric thresholds are selected as $k_{V,L}(t) = 1.5e^{-0.08t} + 0.5$, $k_{V,H}(t) = 0.4e^{-0.08t} + 0.1$, $k_{h,L}(t) = 1.5e^{-0.08t} + 0.5$, $k_{h,H}(t) = 0.2e^{-0.08t} + 0.1$, $k_{\gamma,L}(t) = k_{\alpha,L}(t) = k_{Q,L}(t) = 0.05e^{-0.08t} + 0.05$, and $k_{\gamma,H}(t) = k_{\alpha,H}(t) = k_{Q,H}(t) = 0.1e^{-0.08t} + 0.1$. The initial values of $[V, h, \gamma, \alpha, Q]^\top$ are chosen as $[7699\,\mathrm{ft/s}, 84999\,\mathrm{ft}, 0\,\mathrm{deg}, 1.6325\,\mathrm{deg}, 0\,\mathrm{deg/s}]^\top$, and the initial values of $[\eta_1, \dot{\eta}_1, \eta_2, \dot{\eta}_2]^\top$ are selected as $[0.9700, 0, 0.7967, 0]^\top$.

Simulation results are shown in Figs. 4-5. Fig. 4 (a)-(b) reveal that, in comparison with CICC and CIUC, the proposed control formulation leads to a quicker convergence speed with smoother transients and is robust enough not to violate the imposed asymmetric envelope constraints. It can be observed that if the level of uncertainty lies in the interval $[-30\%, 30\%]$, the velocity and altitude curves obtained utilizing PFCC are smoother and maintained within imposed asymmetric constraints. The lower constraint on the velocity results in above Mach 5 curve, which confirms that the HFV was in the hypersonic regime throughout the flight. The altitude trajectory shows that only a small climbing maneuver is maintained by the controller, which indicates that the HFV was in cruise during the flight. It is clear from Fig. 4 (c) that, the designed compensated signals are featured with fixed-time convergence when considering aerodynamic coefficient uncertainties and external disturbances simultaneously. Fig. 4 (d)-(f) reveal that the control inputs and flight states obtained by PFCC are smoother than those of CICC and CIUC, and there is no high frequency oscillation. It can also be noted that PFCC is effective in fast suppressing the sudden high-frequency transients in 200 s due to the introduction of adaptation laws. In addition, to illustrate the tracking performance and evaluate the control energy quantitatively, integral absolute error (IAE), root mean square error (RMSE), and mean absolute control actions (MACA) are introduced as [16]

$$\mathcal{J}_z(\mathrm{IAE}) = \int_{t_0}^{t} |z(\tau)|\mathrm{d}\tau, \quad \mathcal{J}_z(\mathrm{RMSE}) = \sqrt{\frac{1}{t}\int_{t_0}^{t} z^2(\tau)\mathrm{d}\tau},$$

$$\mathcal{J}_u(\mathrm{MACA}) = \frac{1}{t}\int_{t_0}^{t} |u(\tau)|\mathrm{d}\tau, \quad \mathcal{J}_{\dot{u}}(\mathrm{MACA}) = \frac{1}{t}\int_{t_0}^{t} |\dot{u}(\tau)|\mathrm{d}\tau,$$

where $z \in \{z_h, z_V\}$ and $u \in \{\Phi, \delta_e\}$. The calculation results are summarized in Tables 3-4 and Fig. 5. Table 3 and Fig. 5 show that $\mathcal{J}_{z_V}(\mathrm{IAE})$ obtained by PFCC is respectively less than CICC and CIUC by 50.66% and 57.76%, and $\mathcal{J}_{z_h}(\mathrm{IAE})$ obtained by PFCC is respectively less than CICC and CIUC by 7.34% and 19.86%. This indicates that PFCC exhibits less error energy in contrast to CICC and CIUC. Table 4 and Fig. 5 show that $\mathcal{J}_\Phi(\mathrm{MACA})$ obtained by PFCC is respectively less than CICC and CIUC by 50.66% and 57.76%, and $\mathcal{J}_{\delta_e}(\mathrm{MACA})$ obtained by PFCC is respectively less than CICC and CIUC by 7.34% and 19.86%, implying that the control effort of PFCC is smaller than the one of CICC and CIUC.

6. Conclusion

This work presents a novel fixed-time trajectory tracking control formulation for HFVs in the presence of asymmetric envelope constraints and diverse actuator faults. By introducing fixed-time command filters to produce certain command signals and their derivatives,
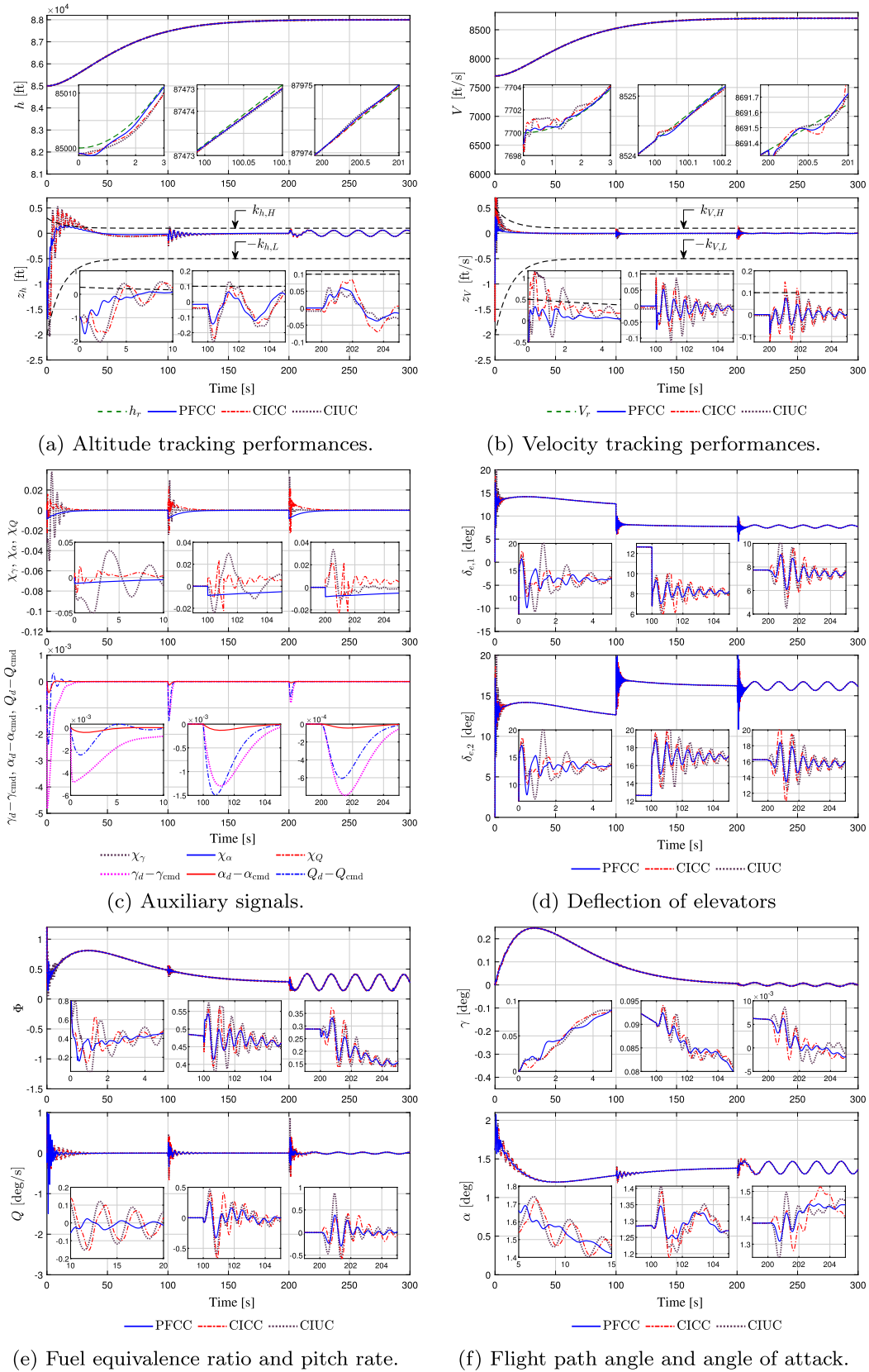
(a) Altitude tracking performances.

(b) Velocity tracking performances.

(c) Auxiliary signals.

(d) Deflection of elevators

(e) Fuel equivalence ratio and pitch rate.

(f) Flight path angle and angle of attack.

Fig. 4. Tracking performances, control inputs and flight states.

a modification is addressed to obviate the explosion of complexity in the backstepping-based design framework. With the aid of a time-varying asymmetric barrier Lyapunov function, satisfactory preselected tracking qualities are guaranteed for flight states via asymmetric envelope constraints. An auxiliary compensating dynamics is integrated into the two-step fault-tolerant control methodology to compen-
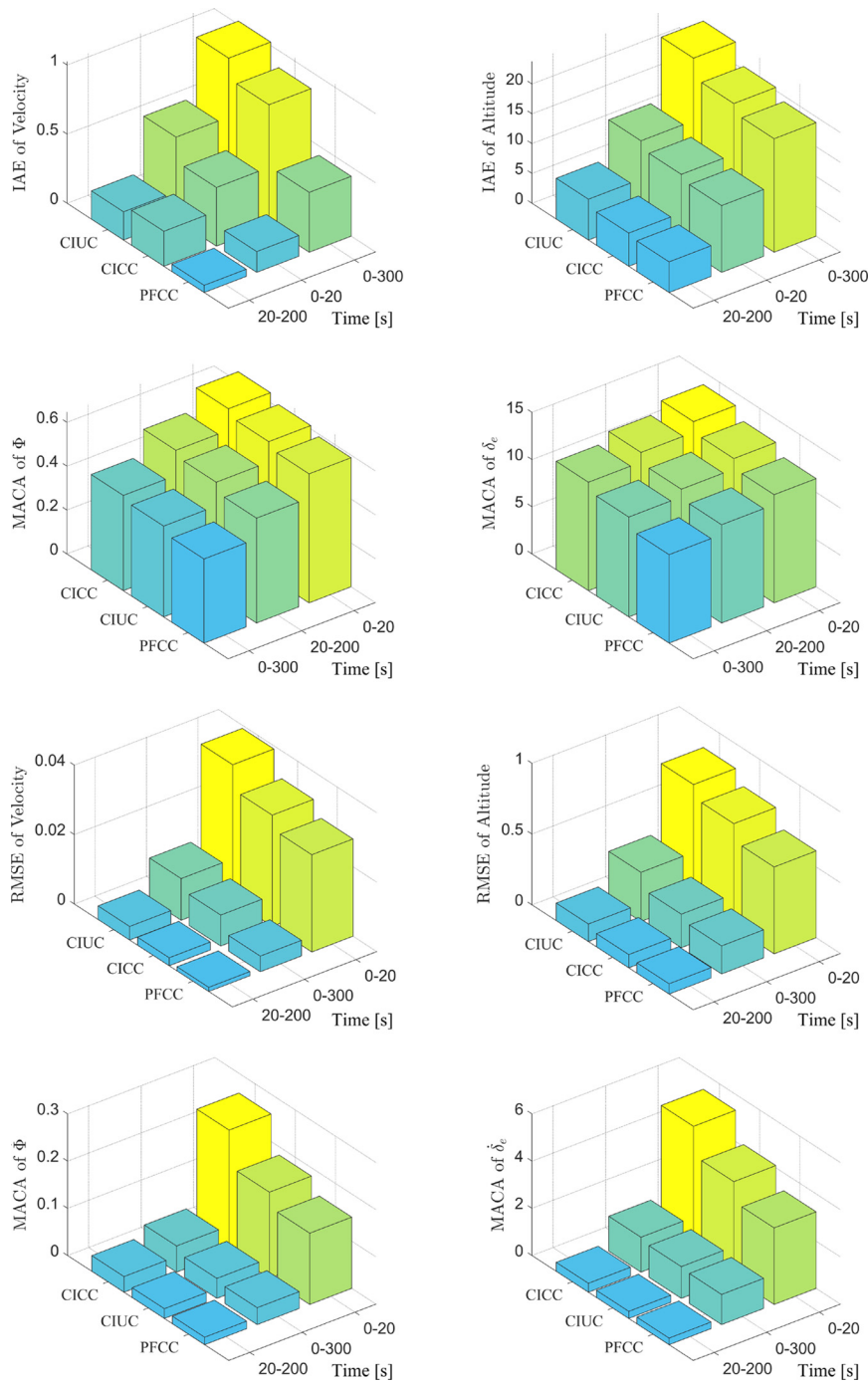
Fig. 5. Performance indices of tracking errors and control inputs.

Table 3
Performance indices of velocity and altitude channels under three methods.

Schemes	Velocity channel		Altitude channel	
	IAE	RMSE	IAE	RMSE
CICC	0.8765	0.0089	20.5314	0.2366
CIUC	1.0239	0.0120	23.7392	0.3468
PFCC	0.4325	0.0045	19.0240	0.1980

sate for the diverse actuator faults (e.g., loss of control effectiveness, bias, and stuck fault). In accordance with the fixed-time stability criterion, it is rigorously proved that both the tracking performance and closed-loop stability can be ensured in fixed time. Comparative simulations have been conducted to highlight the superiorities of the developed method. Future research will be concentrated on visual

Table 4

MACA of control inputs under three methods.

Schemes	Φ	δ_e	$\dot{\Phi}$	$\dot{\delta}_e$
CICC	0.4341	11.4876	0.0554	1.4783
CIUC	0.4139	10.5788	0.0423	1.3442
PFCC	0.3837	9.3749	0.0357	1.2762

simulation and hardware in the loop simulation of the proposed control scheme, as well as the consensus tracking problem for HFV swarm systems [42].

Declaration of competing interest

The authors declare that they have no known competing financial interests or personal relationships that could have appeared to influence the work reported in this paper.

Acknowledgements

Appendix A. Proof of Theorem 1

Step 1. Initially, by combining (4), (7), with (11), the time derivative of $\mathcal{L}_{\mathcal{Z}_V}$ is upper bounded by

$$
\begin{aligned}
\dot{\mathcal{L}}_{\mathcal{Z}_V} \leq{} & \mathcal{Z}_V \varphi_V \zeta_V^\top \boldsymbol{f}_V + \mathcal{Z}_V \varphi_V \zeta_V^\top \boldsymbol{g}_V \sigma_{V,p} \Phi_{\mathrm{cmd}} \\
& + |\mathcal{Z}_V| \varphi_V \vartheta_V - \mathcal{Z}_V \varphi_V \dot{V}_r + \mathcal{Z}_V \varsigma_V .
\end{aligned}
\tag{18}
$$

Substituting (13) into (18), and employing the inequality $0 \leq |q| - \frac{q^2}{\sqrt{q^2+\upsilon^2}} \leq \upsilon$ for $\forall q \in \mathbb{R}$ and $\forall \upsilon > 0$, we arrive at

$$
\begin{aligned}
\dot{\mathcal{L}}_{\mathcal{Z}_V} \leq{} & -\kappa_{V,1} \mathcal{Z}_V^{p+1} - \kappa_{V,2} \mathcal{Z}_V^{q+1} + \mathcal{Z}_V \widetilde{\xi}_\Phi \omega_\Phi \Phi_c + \omega_\Phi \varepsilon \\
& - \widehat{\vartheta}_V \mathcal{Z}_V \varphi_V \mathrm{sg}(\mathcal{Z}_V \varphi_V | \varepsilon) + |\mathcal{Z}_V| \varphi_V \vartheta_V ,
\end{aligned}
\tag{19}
$$

for $|\mathcal{Z}_V| \geq \nu_V$. When $|\mathcal{Z}_V| < \nu_V$, in view of (15), there will be an extra term $\kappa_{V,2} \mathcal{Z}_V^{q+1} + \kappa_{V,2} \sum_{i=1}^{2n-1} l_i \mathcal{Z}_V^{i+1} \nu_V^{q-i}$ in (19). Notice that if $|\mathcal{Z}_V| < \nu_V$, this extra term must be bounded by a small constant ϖ_V. As a result, (19) can be rewritten as

$$
\begin{aligned}
\dot{\mathcal{L}}_{\mathcal{Z}_V} \leq{} & -\kappa_{V,1} \mathcal{Z}_V^{p+1} - \kappa_{V,2} \mathcal{Z}_V^{q+1} + \mathcal{Z}_V \widetilde{\xi}_\Phi \omega_\Phi \Phi_c + \omega_\Phi \varepsilon \\
& - \widehat{\vartheta}_V \mathcal{Z}_V \varphi_V \mathrm{sg}(\mathcal{Z}_V \varphi_V | \varepsilon) + |\mathcal{Z}_V| \varphi_V \vartheta_V + \varpi_V .
\end{aligned}
\tag{20}
$$

Step 2. Similarly and iteratively, substituting (5), (6), and (13) into (11) along the similar lines as (18)-(20), the time derivative of $\mathcal{L}_{\mathcal{Z}_h}$, $\mathcal{L}_{\mathcal{Z}_\gamma}$, $\mathcal{L}_{\mathcal{Z}_\alpha}$, and $\mathcal{L}_{\mathcal{Z}_Q}$ satisfy the inequalities similar to (20), which are omitted here for space limitations.

Step 3. Hereafter, the stabilization of whole system will be investigated. Considering the overall Lyapunov function (16) and invoking (20), the time derivative of $\mathcal{L}$ can be written as

$$
\begin{aligned}
\dot{\mathcal{L}} \leq{} & -\sum_{i \in \Omega_x} \kappa_{i,1} \mathcal{Z}_i^{p+1} - \sum_{i \in \Omega_x} \kappa_{i,2} \mathcal{Z}_i^{q+1} + \sum_{i \in \Omega_x} \vartheta_i \varepsilon + \sum_{i \in \Omega_x} \varpi_i \\
& + \sum_{i \in \Omega_x} \sigma_i \widetilde{\vartheta}_i \widehat{\vartheta}_i + \sum_{j \in \Omega_u} \sigma_j \omega_j \widetilde{\xi}_j \widehat{\xi}_j + \sum_{j \in \Omega_u} \omega_j \varepsilon + 3\varepsilon .
\end{aligned}
\tag{21}
$$

On account of Young's inequality [26], $\widetilde{\vartheta}_i \widehat{\vartheta}_i$ and $\widetilde{\xi}_j \widehat{\xi}_j$ in (21) satisfy $\widetilde{\vartheta}_i \widehat{\vartheta}_i \leq \frac{1}{2} c_i \vartheta_i^2 - \frac{1}{\rho_i} \widetilde{\vartheta}_i^2$ and $\widetilde{\xi}_j \widehat{\xi}_j \leq \frac{1}{2} c_j \xi_j^2 - \frac{1}{\rho_j} \widetilde{\xi}_j^2$. On this basis, (21) can be rewritten as

$$
\dot{\mathcal{L}} \leq -\sum_{i \in \Omega_x} \kappa_{i,1} \mathcal{Z}_i^{p+1} - \sum_{i \in \Omega_x} \kappa_{i,2} \mathcal{Z}_i^{q+1} - \sum_{i \in \Omega_x} \frac{1}{\rho_i} \sigma_i \widetilde{\vartheta}_i^2 - \sum_{j \in \Omega_u} \frac{1}{\rho_j} \sigma_j \omega_j \widetilde{\xi}_j^2 + \mathcal{C}_0 ,
\tag{22}
$$

where $\mathcal{C}_0 = \sum_{i \in \Omega_x} (\frac{1}{2} c_i \sigma_i \vartheta_i^2 + \vartheta_i \varepsilon + \varpi_i) + \sum_{j \in \Omega_u} (\omega_j \varepsilon + \frac{1}{2} c_j \sigma_j \omega_j \xi_j^2) + 3\varepsilon$.

From Lemma 2, there exist inequalities $\left(\frac{\widetilde{\vartheta}_i^2}{2\rho_i}\right)^{\frac{q+1}{2}} \leq \frac{1}{2\rho_i} \widetilde{\vartheta}_i^2 + \frac{1-q}{2} \left(\frac{2}{1+q}\right)^{-\frac{1+q}{1-q}}$ and $\left(\frac{\omega_j \widetilde{\xi}_j^2}{2\rho_j}\right)^{\frac{q+1}{2}} \leq \frac{1}{2\rho_j} \omega_j \widetilde{\xi}_j^2 + \frac{1-q}{2} \left(\frac{2}{1+q}\right)^{-\frac{1+q}{1-q}}$. Incorporating these inequalities into (22) yields

$$
\begin{aligned}
\dot{\mathcal{L}} \leq{} & -\sum_{i \in \Omega_x} \frac{\sigma_i}{2\rho_i} \widetilde{\vartheta}_i^2 - \sum_{j \in \Omega_u} \frac{\sigma_j \omega_j}{2\rho_j} \widetilde{\xi}_j^2 - \mathcal{C}_p \mathcal{L}^{\frac{p+1}{2}} - \mathcal{C}_q \mathcal{L}^{\frac{q+1}{2}} \\
& + \sum_{i \in \Omega_x} \sigma_i \left(\frac{\widetilde{\vartheta}_i^2}{2\rho_i}\right)^{\frac{p+1}{2}} + \sum_{j \in \Omega_u} \sigma_j \left(\frac{\omega_j \widetilde{\xi}_j^2}{2\rho_j}\right)^{\frac{p+1}{2}} + \mathcal{C}_1 ,
\end{aligned}
\tag{23}
$$

with $\mathcal{C}_p = \min\{2^{\frac{p+1}{2}}\kappa_{i,1}, \sigma_i, \sigma_j\}$, $\mathcal{C}_q = \min\{2^{\frac{q+1}{2}}\kappa_{i,2}, \sigma_i, \sigma_j\}$, and $\mathcal{C}_1 = \mathcal{C}_0 + \frac{7(1-q)}{2}\left(\frac{2}{1+q}\right)^{-\frac{1+q}{1-q}}$.

Before moving on, let us first assume that there exist two unknown positive constants Θ_{ϑ_i} and Θ_{ξ_j} satisfying $|\widetilde{\vartheta}_i| \leq \Theta_{\vartheta_i}$ and $|\widetilde{\xi}_j| \leq \Theta_{\xi_j}$. Hereafter, the following two cases need to be considered: 1) If $\Theta_{\vartheta_i} < \sqrt{2\rho_i}$ and $\Theta_{\xi_j} < \sqrt{\frac{2\rho_j}{\omega_j}}$, one has $\sigma_i\left(\frac{\widetilde{\vartheta}_i^2}{2\rho_i}\right)^{\frac{p+1}{2}} - \frac{\sigma_i}{2\rho_i}\widetilde{\vartheta}_i^2 < 0$ and $\sigma_j\left(\frac{\omega_j\widetilde{\xi}_j^2}{2\rho_j}\right)^{\frac{p+1}{2}} - \frac{\sigma_j\omega_j}{2\rho_j}\widetilde{\xi}_j^2 < 0$; 2) Otherwise, one has $\sigma_i\left(\frac{\widetilde{\vartheta}_i^2}{2\rho_i}\right)^{\frac{p+1}{2}} - \frac{\sigma_i}{2\rho_i}\widetilde{\vartheta}_i^2 \leq \sigma_i\left(\frac{\Theta_{\vartheta_i}^2}{2\rho_i}\right)^{\frac{p+1}{2}} + \frac{\sigma_i}{2\rho_i}\Theta_{\vartheta_i}^2$ and $\sigma_j\left(\frac{\omega_j\widetilde{\xi}_j^2}{2\rho_j}\right)^{\frac{p+1}{2}} - \frac{\sigma_j\omega_j}{2\rho_j}\widetilde{\xi}_j^2 \leq \sigma_j\left(\frac{\omega_j\Theta_{\xi_j}^2}{2\rho_j}\right)^{\frac{p+1}{2}} + \frac{\sigma_j\omega_j}{2\rho_j}\Theta_{\xi_j}^2$. Summarizing above two cases yields

$$\dot{\mathcal{L}} \leq -\mathcal{C}_p\mathcal{L}^{\frac{p+1}{2}} - \mathcal{C}_q\mathcal{L}^{\frac{q+1}{2}} + \mathcal{C}_2, \tag{24}$$

where $\mathcal{C}_2 = \mathcal{C}_1 + \sum_{i\in\Omega_x}\sigma_i\left(\frac{\Theta_{\vartheta_i}^2}{2\rho_i}\right)^{\frac{p+1}{2}} + \sum_{i\in\Omega_x}\frac{1}{2\rho_i}\sigma_i\Theta_{\vartheta_i}^2 + \sum_{j\in\Omega_u}\sigma_j\left(\frac{\omega_j\Theta_{\xi_j}^2}{2\rho_j}\right)^{\frac{p+1}{2}} + \sum_{j\in\Omega_u}\frac{1}{2\rho_j}\sigma_j\omega_j\Theta_{\xi_j}^2$.

According to (24), it is easily verified that $\mathcal{L}$ is bounded since $\dot{\mathcal{L}} \leq -\mathcal{C}_q\mathcal{L}^{\frac{q+1}{2}} \leq 0$ for $\mathcal{L}^{\frac{p+1}{2}} \geq \frac{\mathcal{C}_2}{\mathcal{C}_p}$. The boundedness of $\mathcal{L}$ implies the boundedness of $\mathcal{Z}_i$, $\widetilde{\vartheta}_i$, and $\widetilde{\xi}_j$, which, combined with the boundedness of $\widehat{\vartheta}_i$ and $\widehat{\xi}_j$ ($i\in\Omega_x$, $j\in\Omega_u$), ensures that the fixed-time control laws (13) and adaptation laws (14) are bounded. Thence, it is concluded that all the signals in velocity dynamics (4) and altitude dynamics (5) are bounded, and the asymmetric envelope constraints will not be violated during operation. In addition, when $\mathcal{L}^{\frac{p+1}{2}} \geq \frac{\mathcal{C}_2}{\mu_0\mathcal{C}_p}$ with $0 < \mu_0 < 1$, one has $\mathcal{C}_2 \leq \mu_0\mathcal{C}_p\mathcal{L}^{\frac{p+1}{2}}$, which gives rise to

$$\dot{\mathcal{L}} \leq -(1-\mu_0)\mathcal{C}_p\mathcal{L}^{\frac{p+1}{2}} - \mathcal{C}_q\mathcal{L}^{\frac{q+1}{2}}. \tag{25}$$

In the light of Lemma 1 and (25), $\mathcal{L}$ will converge to the set $\Omega_{\mathcal{L}} = \left\{\mathcal{L} < \left(\frac{\mathcal{C}_2}{\mu_0\mathcal{C}_p}\right)^{\frac{2}{p+1}}\right\}$ in fixed time with the guaranteed convergence time estimated as follows

$$\mathcal{T}_0 \leq \mathcal{T}_{0,\max} \triangleq \frac{2}{\mathcal{C}_p(1-\mu_0)(p-1)} + \frac{2}{\mathcal{C}_q(1-q)}. \tag{26}$$

Step 4. In what follows, we will show that χ_γ, χ_α, and χ_Q are bounded in a fixed time. Let us start with constructing the Lyapunov function $\mathcal{L}_\chi = \frac{1}{2}\chi_\gamma^2 + \frac{1}{2}\chi_\alpha^2 + \frac{1}{2}\chi_Q^2$ for the compensated systems. According to Lemma 3, the rest of the proof will be divided into two steps.

1) Initially, based on the properties of fixed-time command filter (8), it will be shown that the system states do not escape to infinity during $\forall t \in [0, \mathcal{T}_1]$. Recalling the stability analysis in [41], the estimation errors $\gamma_d - \gamma_{\mathrm{cmd}}$, $\alpha_d - \alpha_{\mathrm{cmd}}$, and $Q_d - Q_{\mathrm{cmd}}$ are bounded, i.e., there exist some positive constants o_γ, o_α, and o_Q satisfying $o_\gamma \geq |\gamma_d - \gamma_{\mathrm{cmd}}|$, $o_\alpha \geq |\alpha_d - \alpha_{\mathrm{cmd}}|$, and $o_Q \geq |Q_d - Q_{\mathrm{cmd}}|$ for $\forall t \in [0, \mathcal{T}_1]$. Thence, differentiating $\mathcal{L}_\chi$ with respect to time obtains

$$\dot{\mathcal{L}}_\chi \leq \Xi_\chi\mathcal{L}_\chi + \Xi_0, \tag{27}$$

where $\Xi_0 = \frac{1}{2}Vo_\gamma^2 + \frac{1}{2}\|\boldsymbol{\zeta}_\gamma\|\|\mathbf{g}_\gamma\|o_\alpha^2 + \frac{1}{2}\|\boldsymbol{\zeta}_\alpha\|\|\mathbf{g}_\alpha\|o_Q^2$, $\Xi_\chi = \max\{\Xi_\gamma, \Xi_\alpha, \Xi_Q\}$ with $\Xi_\gamma = 2V$, $\Xi_\alpha = 2\|\boldsymbol{\zeta}_\gamma\|\|\mathbf{g}_\gamma\| + V$, and $\Xi_Q = \|\boldsymbol{\zeta}_\alpha\|\|\mathbf{g}_\alpha\| + \|\boldsymbol{\zeta}_\gamma\|\|\mathbf{g}_\gamma\|$. Solving inequality (27) obtains $\mathcal{L}_\chi(t) \leq (\mathcal{L}_\chi(0) + \Xi_0/\Xi_\chi)\exp(\Xi_\chi T_1)$ for $\forall t \in [0, \mathcal{T}_1]$, where $\mathcal{L}_\chi(0)$ represents the initial value of $\mathcal{L}_\chi$. As such, it can be derived that all the closed-loop system states will not escape to infinity for $\forall t \in [0, \mathcal{T}_1]$.

2) Then, the fixed-time convergence of the closed-loop system states will be proven in this step. Invoking (9) and setting $c_{\gamma,1}$, $c_{\alpha,1}$, and $c_{Q,1}$ such that $c_{\gamma,1} \geq \frac{1}{2}V$, $c_{\alpha,1} \geq \frac{1}{2}\|\boldsymbol{\zeta}_\gamma\|\|\mathbf{g}_\gamma\| + \frac{1}{2}V$, and $c_{Q,1} \geq \frac{1}{2}\|\boldsymbol{\zeta}_\gamma\|\|\mathbf{g}_\gamma\|$, the following inequality holds:

$$\dot{\mathcal{L}}_\chi \leq -\varpi_1\mathcal{L}_\chi^2 - \varpi_2\sqrt{\mathcal{L}_\chi}, \tag{28}$$

with $\varpi_1 = \min\{4c_{\gamma,2}, 4c_{\alpha,2}, 4c_{Q,2}\}$ and $\varpi_2 = \min\{\sqrt{2}\ell_\gamma, \sqrt{2}\ell_\alpha, \sqrt{2}\ell_Q\}$. In view of (28) and Lemma 1, χ_γ, χ_α, and χ_Q will converge to zero within a fixed time satisfying

$$t \geq \mathcal{T}_2 = \mathcal{T}_1 + \mathcal{T}_{0,\max} \triangleq \mathcal{T}_1 + \frac{1}{\varpi_1} + \frac{2}{\varpi_2}. \tag{29}$$

To sum up, recalling (25), Lemma 1, and the construction of $\mathcal{L}$ in (16), it is straightforward to deduce that

$$|\mathcal{Z}_h| < \sqrt{2\left(\frac{\mathcal{C}_2}{\mu_0\mathcal{C}_p}\right)^{\frac{2}{p+1}}}, \quad |\mathcal{Z}_V| < \sqrt{2\left(\frac{\mathcal{C}_2}{\mu_0\mathcal{C}_p}\right)^{\frac{2}{p+1}}}, \tag{30}$$

for $\forall t \geq \max\{\mathcal{T}_0, \mathcal{T}_2\}$. This further indicates that $\mathcal{Z}_h$ and $\mathcal{Z}_V$ converge into a disc region with radius $\sqrt{2\left(\frac{\mathcal{C}_2}{\mu_0\mathcal{C}_p}\right)^{\frac{2}{p+1}}}$ in fixed time. $\square$

References

[1] H. An, Q. Wu, G. Wang, Z. Guo, C. Wang, Simplified longitudinal control of air-breathing hypersonic vehicles with hybrid actuators, Aerosp. Sci. Technol. 104 (Sept. 2020) 105936.

[2] K. An, Z. Guo, X. Xu, W. Huang, A framework of trajectory design and optimization for the hypersonic gliding vehicle, Aerosp. Sci. Technol. 106 (Nov. 2020) 106110.

[3] Z. Dong, Y. Li, M. Lv, R. Zuo, Adaptive accurate tracking control of HFVs in the presence of dead-zone and hysteresis input nonlinearities, Chin. J. Aeronaut. 34 (5) (May 2021) 642–651.

[4] L. Fiorentini, A. Serrani, Adaptive restricted trajectory tracking for a non-minimum phase hypersonic vehicle model, Automatica 48 (7) (Jul. 2012) 1248–1261.

[5] R. Zuo, Y. Li, M. Lv, X. Wang, Z. Liu, Realization of trajectory precise tracking for hypersonic flight vehicles with prescribed performances, Aerosp. Sci. Technol. 111 (Apr. 2021) 106554.

[6] H. Qiao, H. Meng, M. Wang, W. Ke, J. Sun, Adaptive control for hypersonic vehicle with input saturation and state constraints, Aerosp. Sci. Technol. 84 (Jan. 2019) 107–119.

[7] J.T. Parker, A. Serrani, S. Yurkovich, M.A. Bolender, D.B. Doman, Control-oriented modeling of an air-breathing hypersonic vehicle, J. Guid. Control Dyn. 30 (3) (2007) 856–869.

[8] Y. Shen, W. Huang, L. Yan, T. Zhang, Constraint-based parameterization using FFD and multi-objective design optimization of a hypersonic vehicle, Aerosp. Sci. Technol. 100 (May 2020) 105788.

[9] Y. Wang, T. Chao, S. Wang, M. Yang, Byrnes-Isidori-based dynamic sliding-mode control for nonminimum phase hypersonic vehicles, Aerosp. Sci. Technol. 95 (Dec. 2019) 105478.

[10] X. Wang, E.V. Kampen, Q. Chu, P. Lu, Incremental sliding-mode fault-tolerant flight control, J. Guid. Control Dyn. 42 (2) (Nov. 2019) 244–259.

[11] H. Xu, M. Mirmirani, P. Ioannou, Adaptive sliding mode control design for a hypersonic flight vehicle, J. Guid. Control Dyn. 27 (Sept. 2004) 829–838.

[12] Q. Hu, C. Wang, Y. Li, J. Huang, Adaptive control for hypersonic vehicles with time-varying faults, IEEE Trans. Aerosp. Electron. Syst. 54 (3) (Jun. 2018) 1442–1455.

[13] B. Xu, R. Qi, B. Jiang, Adaptive fault-tolerant control for HSV with unknown control direction, IEEE Trans. Aerosp. Electron. Syst. 55 (6) (Dec. 2019) 2743–2758.

[14] X. Wang, E.V. Kampen, Q. Chu, P. Lu, Stability analysis for incremental nonlinear dynamic inversion control, J. Guid. Control Dyn. 42 (5) (Mar. 2019) 1116–1129.

[15] X. Bu, G. He, K. Wang, Tracking control of air-breathing hypersonic vehicles with non-affine dynamics via improved neural back-stepping design, ISA Trans. 75 (2018) 88–100.

[16] M. Lv, Y. Li, W. Pan, S. Baldi, Finite-time fuzzy adaptive constrained tracking control for hypersonic flight vehicles with singularity-free switching, IEEE/ASME Trans. Mechatron. (Jun. 2021), https://doi.org/10.1109/TMECH.2021.3090509 (early access).

[17] J. Chang, Z. Guo, J. Cieslak, W. Chen, Integrated guidance and control design for the hypersonic interceptor based on adaptive incremental backstepping technique, Aerosp. Sci. Technol. 89 (Jun. 2019) 318–332.

[18] I. Kanellakopoulos, P.V. Kokotovic, A.S. Morse, Systematic design of adaptive controllers for feedback linearizable systems, IEEE Trans. Autom. Control 36 (11) (1991) 1241–1253.

[19] M. Krstic, I. Kanellakopoulos, P. Kokotovic, Nonlinear and Adaptive Control Design, Wiley, New York, 1995.

[20] R. Zuo, X. Dong, Y. Liu, Z. Liu, W. Zhang, Adaptive neural control for MIMO pure-feedback nonlinear systems with periodic disturbances, IEEE Trans. Neural Netw. Learn. Syst. 30 (6) (Jun. 2019) 1756–1767.

[21] H.K. Khalil, Nonlinear Systems, 3rd ed., Prentice Hall, Englewood Cliffs, NJ, 2002.

[22] D. Swaroop, J.K. Hedrick, P.P. Yip, J.C. Gerdes, Dynamic surface control for a class of nonlinear systems, IEEE Trans. Autom. Control 45 (2000) 1893–1899.

[23] J.A. Farrell, M. Polycarpou, M. Sharma, W.J. Dong, Command filtered backstepping, IEEE Trans. Autom. Control 54 (2009) 1391–1395.

[24] W. Dong, J.A. Farrell, M. Polycarpou, V. Djapic, M. Sharma, Command filtered adaptive backstepping, IEEE Trans. Control Syst. Technol. 20 (2012) 566–580.

[25] J. Yu, L. Zhao, H. Yu, C. Lin, Barrier Lyapunov functions-based command filtered output feedback control for full-state constrained nonlinear systems, Automatica 105 (2019) 71–79.

[26] J. Yu, P. Shi, L. Zhao, Finite-time command filtered backstepping control for a class of nonlinear systems, Automatica 92 (2018) 173–180.

[27] Y. Li, Finite time command filtered adaptive fault tolerant control for a class of uncertain nonlinear systems, Automatica 106 (2019) 117–123.

[28] Y. Li, T. Yang, S. Tong, Adaptive neural networks finite-time optimal control for a class of nonlinear systems, IEEE Trans. Neural Netw. Learn. Syst. 31 (11) (Nov. 2020) 4451–4460.

[29] Y. Li, K. Li, S. Tong, Adaptive neural network finite-time control for multi-input and multi-output nonlinear systems with the powers of odd rational numbers, IEEE Trans. Neural Netw. Learn. Syst. 31 (7) (Jul. 2020) 2532–2543.

[30] J. Sun, Z. Pu, J. Yi, Z. Liu, Fixed-time control with uncertainty and measurement noise suppression for hypersonic vehicles via augmented sliding mode observers, IEEE Trans. Ind. Inform. 16 (2020) 1192–1203.

[31] A. Polyakov, Nonlinear feedback design for fixed-time stabilization of linear control systems, IEEE Trans. Autom. Control 57 (2012) 2106–2110.

[32] K.P. Tee, S.S. Ge, Barrier Lyapunov functions for the control of output-constrained nonlinear systems, Automatica 45 (2009) 918–927.

[33] B. Xu, Z.K. Shi, F.C. Sun, W. He, Barrier Lyapunov function based learning control of hypersonic flight vehicle with AOA constraint and actuator faults, IEEE Trans. Cybern. 49 (3) (Mar. 2019) 1047–1057.

[34] X. Bu, Envelope-constraint-based tracking control of air-breathing hypersonic vehicles, Aerosp. Sci. Technol. 95 (2019) 105429.

[35] Y. Li, Y. Liu, S. Tong, Observer-based neuro-adaptive optimized control for a class of strict-feedback nonlinear systems with state constraints, IEEE Trans. Neural Netw. Learn. Syst. (Jan. 2021), https://doi.org/10.1109/TNNLS.2021.3051030 (early access).

[36] K.P. Tee, S.S. Ge, Control of state-constrained nonlinear systems using integral barrier Lyapunov functionals, in: 51st IEEE Conference on Decision and Control, 2012, pp. 3239–3244.

[37] J. Xia, J. Zhang, W. Sun, B. Zhang, Z. Wang, Finite-time adaptive fuzzy control for nonlinear systems with full state constraints, IEEE Trans. Syst. Man Cybern. Syst. 49 (7) (Jul. 2019) 1541–1548.

[38] M. Lv, W. Yu, J. Cao, S. Baldi, Consensus in high-power multi-agent systems with mixed unknown control directions via hybrid Nussbaum-based control, IEEE Trans. Cybern. (Nov. 2020), https://doi.org/10.1109/TCYB.2020.3028171 (early access).

[39] C. Qian, W. Lin, A continuous feedback approach to global strong stabilization of nonlinear systems, IEEE Trans. Autom. Control 46 (2001) 1061–1079.

[40] M. Lv, W. Yu, J. Cao, S. Baldi, A separation-based methodology to consensus tracking of switched high-order nonlinear multi-agent systems, IEEE Trans. Neural Netw. Learn. Syst. (Apr. 2021), https://doi.org/10.1109/TNNLS.2021.3070824 (early access).

[41] M.V. Basin, P. Yu, Y.B. Shtessel, Hypersonic missile adaptive sliding mode control using finite- and fixed-time observers, IEEE Trans. Ind. Electron. 65 (1) (Jan. 2018) 930–941.

[42] M. Lv, B. De Schutter, C. Shi, S. Baldi, Logic-based distributed switching control for agents in power chained form with multiple unknown control directions, Automatica (2021), in press.